Study on properties of Al_2O_3-13wt.% TiO_2 coating sprayed by atmospheric plasma spraying

J. J. Li [a,*], Y. F. Zhang [b], F. Li [a], Q. Q.Yu [a], W. X. Du [a], T. W. Qiu [a], C. L. Gao [a], G. S. Chen [c]

[a] *School of Mechanical Engineering, Shandong Huayu University of Technology, Dezhou, Shandong, 253000, PR China*

[b] *School of Mechanical Engineering, Qilu University of Technology (Shandong Academy of Sciences), Jinan, Shandong, 250353, PR China*

[c] *Beijing Jike Guochuang Lightweight Science Research Institute Co., Ltd. Beijing, 100000, PR China*

The Al_2O_3-13wt.% TiO_2 coatings were fabricated on 304 steel by atmospheric plasma spraying (APS). The properties of coating were analyzed. The results show that the Al_2O_3-13wt.% TiO_2 coating exhibits a typical lamellar structure with some microcracks and pores, which are attributed to the nature of APS. The coating presents a mechanical bond with the substrate and bonds well. Unlike the physical phase of the Al_2O_3-13wt.% TiO_2 powder, the physical phase of the coating was increased with γ-Al_2O_3 and Al_2TiO_5 phases. The surface roughness value of the Al_2O_3-13wt.% TiO_2 coating is 5.07 μm and the coating has a relatively smooth surface. The average hardness of Al_2O_3-13wt.% TiO_2 coating is 801 $HV_{0.2}$, but its hardness measurement value has a certain fluctuation. The Al_2O_3-13wt.% TiO_2 coating has good corrosion resistance compared to the substrate.

(Received March 29, 2025; Accepted July 29, 2025)

Keywords: Atmospheric plasma spraying, Al_2O_3-13wt.% TiO_2 coating, Corrosion resistance

1. Introduction

With industrial modernization, the performance requirements for metallic materials are increasing as they are widely used in diverse and demanding environments. Therefore, metal materials need to be resistant to high-temperature oxidation, thermal shock, abrasion, corrosion, erosion, and thermal insulation[1-3]. Coating the surface of the material is especially necessary to ensure the integrity of the substrate, and this field has seen rapid development. Metal samples treated with coating technology not only maintain the inherent strength and toughness of the metal matrix, but also add new performance characteristics such as resistance to abrasion and corrosion, thus enhancing the material's performance, life and scope of application[4]. Metal-based ceramic coatings are now common in various fields[5-8]. Ceramic coatings are formed by thermal spraying[9,

* Corresponding author: lijunjie202209@163.com

https://doi.org/10.15251/DJNB.2025.203.869

[10]and other techniques[11, 12] to form one or more layers of coatings on the surface of the substrate, and after high-temperature sintering, the substrate material reacts and combines with the coatings so that they are tightly connected. Ceramic coating is easy to control the degree of thinness and thickness, but also according to the use of performance and the use of environmental needs to deploy the composition of the coating, ceramic coatings have other coating materials can not be compared with the characteristics of the material, therefore greatly expanding the scope of application of the material[13].

The hardness of alumina ceramics is very high, and its Mohs hardness can reach 9. Alumina ceramic materials have a high melting point, stable high-temperature chemical properties, low thermal conductivity, and their performance ranks second among the common high-temperature-resistant ceramic coating materials, after zirconium oxide[14]. Alumina ceramics have a higher electrical resistivity and dielectric constant than other materials, as well as a dielectric strength of 1069 V/ 0. 1 mm, so alumina is often used as an insulating coating material. Alumina ceramics, as a neutral oxide, are known for their excellent light and high-temperature radiation reflectance properties despite their relatively low thermal emissivity. This property makes alumina ceramics have a wide application prospect in the field of artificial satellites, especially in scenarios requiring resistance to sunlight exposure as well as backlit thermal insulation coatings[15, 16]. Passivated aluminum oxide coatings have the disadvantage of high porosity. In order to improve its corrosion resistance and insulating properties, it is often treated by sealing technology in practical production.

Other oxide materials are added to the alumina material so that a series of Al_2O_3-based alumina composites can be produced[17]. Currently, alumina composites widely used in thermal spray technology include Al_2O_3-TiO_2, Al_2O_3-SiO_2 and Al_2O_3-MgO[18-20]. The application of these composites allows for the preparation of coatings with even better performance, significantly enhancing the key properties of pure Al_2O_3 ceramics, such as corrosion resistance, thermal and electrical insulation, to meet the needs of a wider range of practical applications.

If high hardness, wear resistance and chemical resistance are required, pure aluminum-based powders should be used. High purity alumina powders are also the most suitable candidates for electrical and biomedical applications[21]. Al_2O_3 can also be used as an abrasion-resistant coating at high temperatures, and as a corrosion-resistant coating against corrosion of molten metals and slag, demonstrating excellent corrosion resistance[22].

Compared with pure Al_2O_3 material, Al_2O_3-TiO_2 has good bonding and toughness, greater impact load strength and hardness, lower relative coefficient of friction, and excellent abrasion and corrosion resistance[16, 23]. $A1_2O_3$-3wt.% TiO_2 is commonly used to prepare a range of high-performance coatings, $A1_2O_3$-3wt.% TiO_2 coatings have higher high fracture toughness than pure alumina coatings, but still lower than Al_2O_3-13wt.% TiO_2 coatings. Al_2O_3-40wt.% TiO_2 coatings have the highest fracture toughness, but they have lower hardness, abrasion resistance, and chemical resistance than Al_2O_3-13wt.% TiO_2 coatings. Alternatively, Al_2O_3-40wt.% TiO_2 can be used to prepare coatings for use in environments up to 540°C. These coatings are resistant to corrosive wear from most dilute acids (except sulfuric and phosphoric acids) and dilute alkaline solutions[24].

However, Al_2O_3-13wt.% TiO_2 composites are particularly suitable for wear coatings used in environments up to 540 °C. This composite exhibits excellent performance in terms of resistance to cavitation, wear corrosion, and particle erosion[25]. Al_2O_3-13wt.% TiO_2 coatings are

widely used in automotive components, such as engine blocks, valves, pistons and fuel pumps, etc[26]. Therefore, in this paper, the Al_2O_3-13wt.% TiO_2 coatings were prepared by APS, and the micro-morphology, phase detection, Vickers hardness, surface roughness and corrosion resistance of the Al_2O_3-13wt.% TiO_2 coating were studied.

2. Experiment procedures

2.1. Coating deposition

Commercially available Al_2O_3-13wt.% TiO_2 powder (15-65μm, AT13) was used to prepare the coating. The composition of Al_2O_3-13wt.% TiO_2 powder is presented in Table 1. Use of Ni-Al coating as a bond coating. The specimen substrate is 304 steel plate, and the specimen size is 10 mm×10 mm×2 mm. 60 mesh white corundum was used for sand blasting before spraying. Spraying with ZB-80K atmospheric plasma spraying system. The spraying parameters of Ni-Al coating and Al_2O_3-13wt.% TiO_2 coating is presented in Table 2. The coating structure is illustrated in Fig. 1. The thickness of the Al_2O_3-13wt.% TiO_2 coating is usually larger than Ni-Al coating, which protects the substrate[27-29].

Table 1. Chemical composition of Al_2O_3-13wt. % TiO_2 powder (wt. %).

SiO_2	Fe_2O_3	MgO	CaO	TiO_2	Al_2O_3
0.5	0.2	0.2	0.1	13	balance

Table 2. Spraying process parameters for coatings.

Samples	Voltage (V)	Current (A)	Spray distance (mm)	Argon flow (L/min)	Hydrogen flow (L/min)	Power feed rate (RPM)
Ni-Al	70	598	150	34	3	6
Al_2O_3-13wt. % TiO_2	68	700	135	38	3	7.4

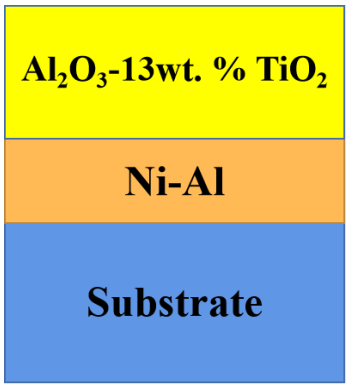

Fig. 1. Schematic diagram of coating structure.

2.2. Material characterization

The surface and cross-section of the Al_2O_3-13wt.% TiO_2 coating were observed by a GeminiSEM 500 scanning electron microscope, and thus the morphology and microstructure were analyzed. A SmartlabSE X-ray diffractometer was used to determine the phase composition. Surface roughness of the Al_2O_3-13wt.% TiO_2 coating was determined using a KC-XI000 laser spectral confocal microscope. Measurement of Vickers hardness of substrates, Ni-Al coatings and Al_2O_3-13wt.% TiO_2 coatings by a HXD-1000TMC micro-Vickers hardness tester. Hardness measurements of the substrate were averaged over 5 points, and hardness measurements of the Ni-Al coating and the Al_2O_3-13wt.% TiO_2 coating were averaged over 10 points. Corrosion test of Al_2O_3-13wt.% TiO_2 coating was performed using electrochemical workstation (CHI660E) in 3.5wt % NaCl solution at room temperature.

3. Results and discussion

3.1. Powder characteristics

Fig. 2 displays the SEM image of Al_2O_3-13wt.% TiO_2 powder, which was produced by agglomerate sintering with irregular appearance morphology and angularity. The size distribution of Al_2O_3-13wt.% TiO_2 powder is shown in Fig. 3, and the size distribution is in the range of 13-63 μm. It has excellent flowability，deposition efficiency is significantly improved even at high powder feed rates. As a result, the use of this powder produces coatings with excellent performance, while offering potential cost benefits in terms of reduced processing time. The purpose of drying the powder before spraying is to increase the fluidity of the powder. The XRD pattern of Al_2O_3-13wt.% TiO_2 powder is shown in Fig. 4. The main forming phases in the Al_2O_3-13wt.% TiO_2 powder are α-Al_2O_3, Rutile-TiO_2 phase and a small amount of Al_2TiO_5 phase.

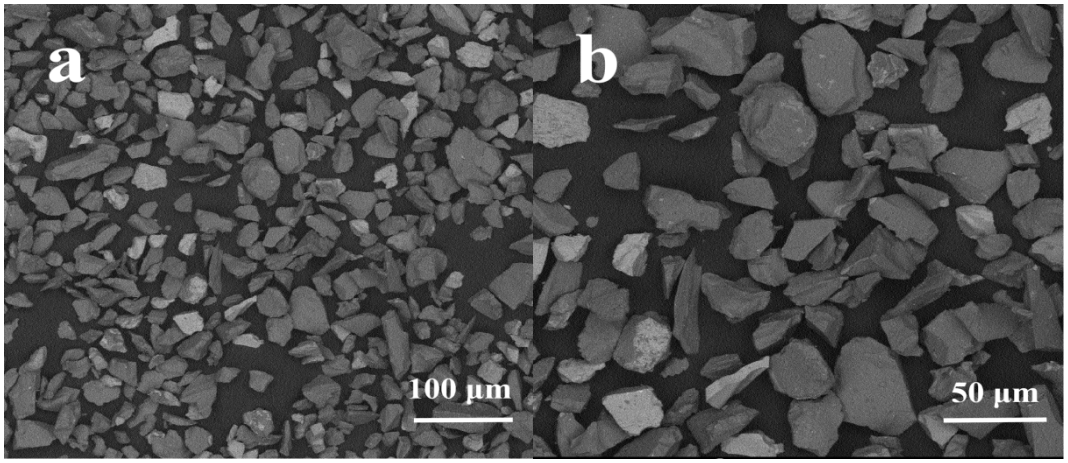

Fig. 2. SEM image of Al_2O_3-13wt.% TiO_2 powder.

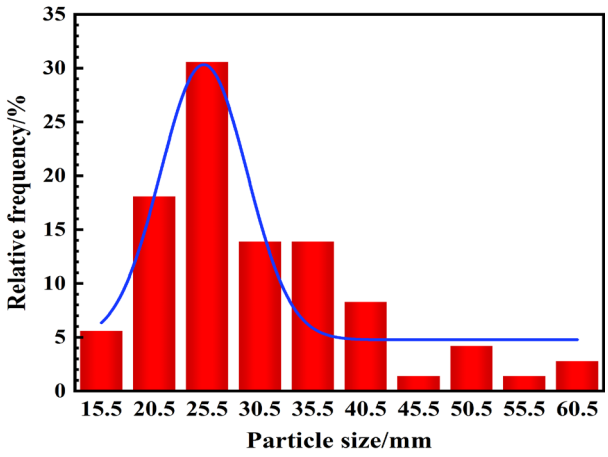

Fig. 3. Particle size distribution of Al_2O_3-13wt.% TiO_2 powders.

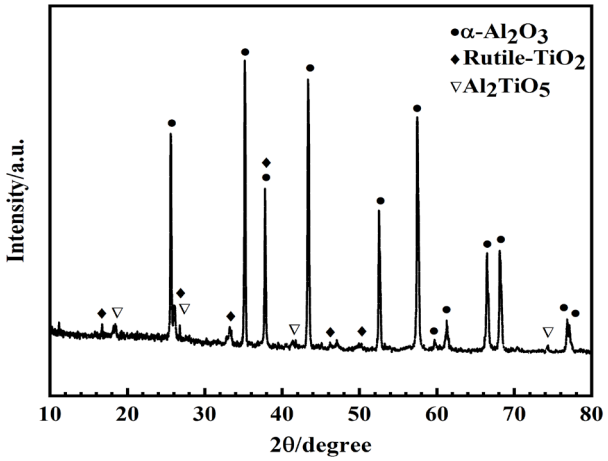

Fig. 4. XRD pattern of Al_2O_3-13wt.% TiO_2 powder.

3.2. Coating characteristics

The surface morphologies of the Al_2O_3-13wt.% TiO_2 coating are presented in Fig. 5. The Al_2O_3-13wt.% TiO_2 coating is homogeneous and consistent, and its surface morphology consists of fully molten regions, partially molten regions, pores and cracks. The reason for this complex structure can be explained by the fact that the Al_2O_3-13wt.% TiO_2 powder was transported to the surface by the plasma in a few seconds, and some of the particles were completely melted and deposited on the surface as cleavage forms. However, some particles remained on the surface as unmelted particles.

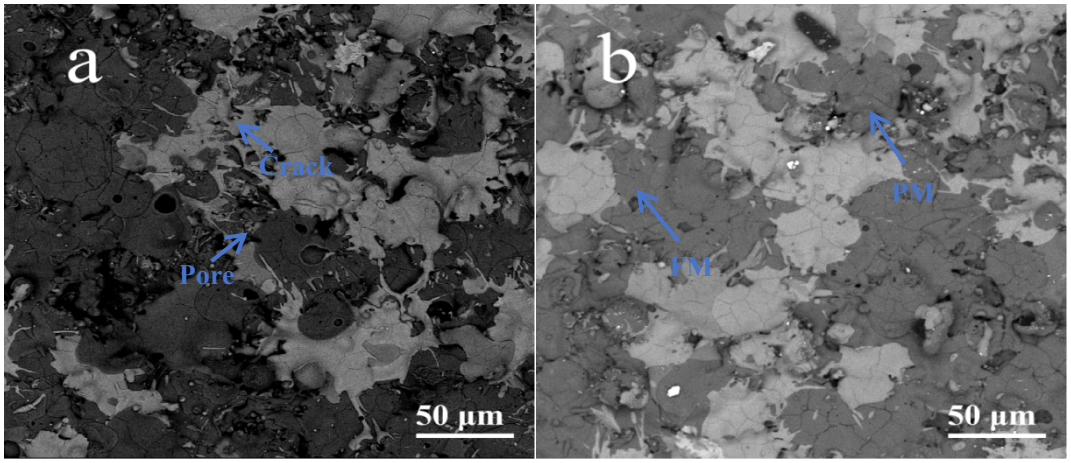

Fig. 5. Surface morphologies of Al_2O_3-13wt.% TiO_2 coating.

Fig. 6 presents the SEM diagrams of cross-sectional morphology of the Al_2O_3-13wt.% TiO_2 coatings. This shows that the Al_2O_3-13wt.% TiO_2 coatings all have the typical properties of thermal spray coatings with a typical layer structure. The coating adheres to the substrate without large gaps, but still has some holes. The coating has no major defects and adheres well to the substrate. In the high magnification images, the Al_2O_3-13wt.% TiO_2 coating was observed to have a characteristic undulating microstructure of unmelted particles, pores and microcracks. Al_2O_3 and TiO_2 are uniformly distributed over all cross sections of Fig. 6. The bright and dark areas in the figure correspond to Al_2O_3 and TiO_2, respectively.

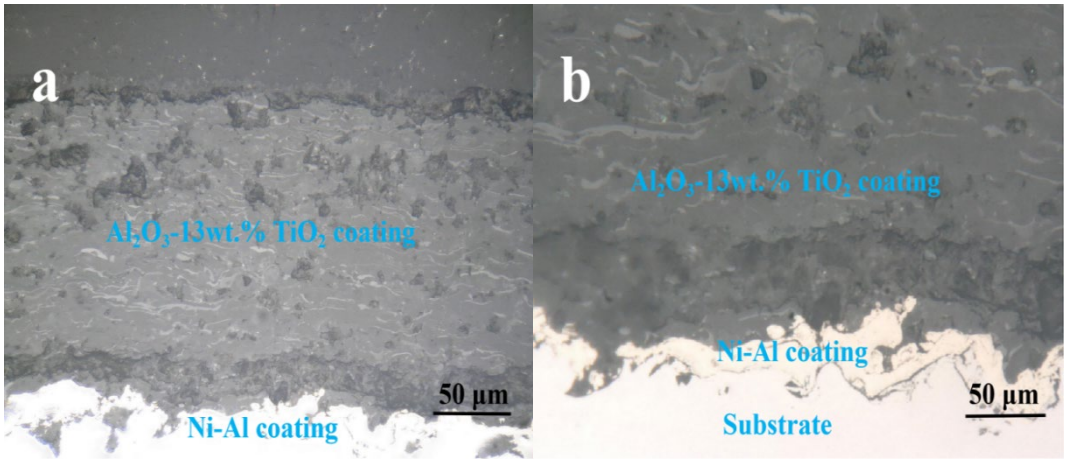

Fig. 6. SEM diagrams of cross-sectional morphology of Al_2O_3-13wt.% TiO_2 coating

Crystal peaks corresponding to γ-Al_2O_3 were found in the XRD pattern (As seen in Fig. 7). This can be attributed to the fact that γ-Al_2O_3 is a substable phase. γ-Al_2O_3 is the main crystalline phase. When the power is melted by the high temperature of the plasma flame, the γ-Al_2O_3 phase nucleates and grows due to rapid cooling. However, the γ-Al_2O_3 phase that has been formed is not a stable phase at high temperatures. γ-Al_2O_3 is a cubic crystal system, which is formed by rapid cooling at temperatures above 1000°C. The γ-Al_2O_3 phase has been formed by the rapid cooling of

the γ-Al_2O_3 phase at temperatures above 1000°C, which is a very high temperature. The formation of γ-Al_2O_3 then increases the porosity of the Al_2O_3-13wt.% TiO_2 coatings due to the presence of γ-Al_2O_3 weaving, which is selectively oriented. However, as soon as the porosity is high, many of the coating's properties are affected, such as corrosion and abrasion resistance. Therefore, the less γ-Al_2O_3 present in the coating, the better, so that the coating will have better performance in use. In addition, the reactivity of the constituent elements increased at high temperatures. As a result, the Al_2TiO_5 phase is formed due to the reaction of the alumina phase and the titanium dioxide phase.

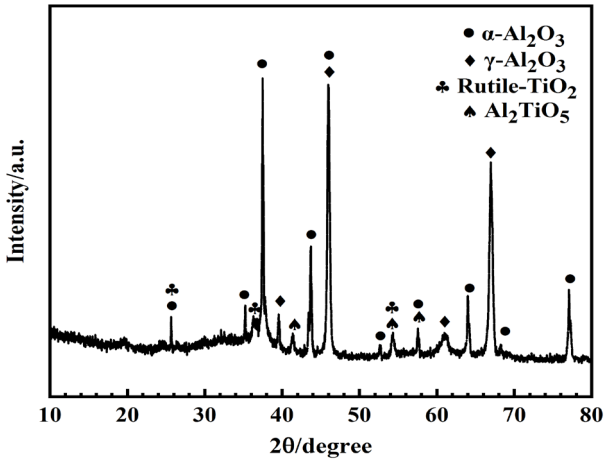

Fig. 7. XRD pattern of Al_2O_3-13wt.% TiO_2 coating.

The surface roughness exhibited by the Al_2O_3-13wt.% TiO_2 coating is illustrated in Fig. 8, and the surface roughness value of the Al_2O_3-13wt.% TiO_2 coating is 5.07 μm. In this case, the agglomerated and non-sintered forms of the sprayed powder are more easily broken, leading to lower Ra values. From Fig. 8, it can be seen that the coating is thinner at the left corner of the coating. The thickness of the Al_2O_3-13wt.% TiO_2 coating after spraying is between 150-200 μm. The cause of this phenomenon gun moving speed is not uniform, the error is large, the center of the specimen is not aligned with the gun. This is because coatings obtained by plasma spraying usually contain a porous structure of more than 10 percent and partially melted or unmelted areas.

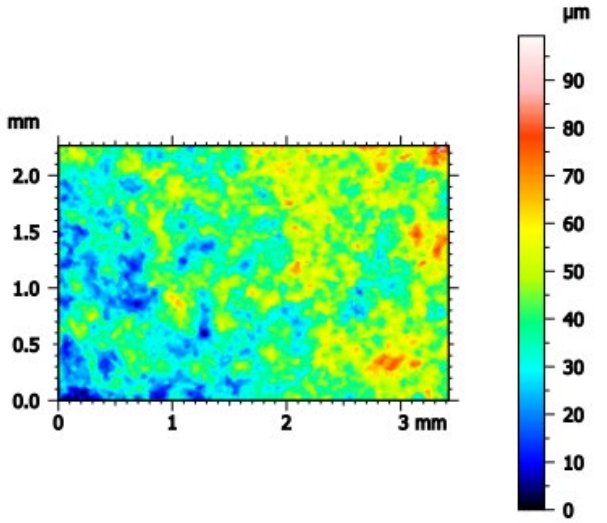

Fig. 8. Confocal microscopy images of Al_2O_3-13wt.% TiO_2 coatings.

Before measuring the hardness，the coating specimens were cold set and polished prior to the measurement, and the measurements were made on the coating cross section, with the test points selected along the horizontal direction of the coating. The Vickers measurements of the Al_2O_3-13wt.% TiO_2 coatings are displayed in Table 3, and the average Vickers hardness value of the Al_2O_3-13wt.% TiO_2 coatings is 801 $HV_{0.2}$. The microhardness of coatings containing alumina plus titanium dioxide is lower than that of alumina, independently of the process parameters, and the increase in the value of titanium dioxide leads to a decrease in the microhardness value. The results show that the effect of phase composition overcomes the effect of porosity. Regardless of the spraying method, the α-Al_2O_3 phase content of the Al_2O_3-13wt.% TiO_2 coatings decreased after spraying. The hardness of Al_2TiO_5 and rutile TiO_2 is lower than that of α-Al_2O_3 phase.

Table 3. Vickers hardness values of Al_2O_3-13wt.% TiO_2 coatings.

Coating	Vickers hardness values/HV										Average value/HV
AT13 coating	726	865	780	780	820	823	840	790	788	798	801

Fig. 9 shows the microhardness gradient distribution from the substrate to the surface coating. As can be seen in Fig. 9, the cross-section average hardness of the AT13 coating is 801 $HV_{0.2}$, which is more than twice the hardness of the 304 steel substrate. The Vickers hardness of the Al_2O_3-13wt.% TiO_2 coatings was significantly increased by APS, due to the high jet temperature, so that the fine grain strengthening could be realized, and therefore the microhardness of the Al_2O_3-13wt.% TiO_2 coatings after spraying was high. Unlike the Ni-Al bonded coating, the microhardness values of the AT13 coating fluctuated considerably. This is due to the fact that the Al_2O_3-13wt.% TiO_2 coating shows a bimodal distribution structure, and the structural difference between the partially molten zone and the fully molten zone in the Al_2O_3-13wt.% TiO_2 coating is large, with lower hardness values in the partially molten zone and higher hardness values in the fully molten zone, which results in the ups and downs of hardness values. The Al_2O_3-13wt.% TiO_2 coating has a laminar structure in the fully molten zone with phase compositions of α-Al_2O_3 and γ-Al_2O_3, while the partially molten zone has a near-sintered state structure, i.e., the melted Al_2TiO_5 matrix is inlaid with unfused α-Al_2O_3 particles, and the average hardness value is lower than that of the fully molten zone due to the looseness of the organization. In conclusion, the reason for the ups and downs of the hardness value of the Al_2O_3-13wt.% TiO_2 coating is mainly that Al_2O_3 undergoes a crystalline transformation in the process of APS, and the hardness value decreases when it is transformed from the α-Al_2O_3 of the original powder to the substable γ-Al_2O_3, which means that the hardness of α-Al_2O_3 is higher than that of γ-Al_2O_3. The more the α-Al_2O_3 amount in the sample, the more favorable the hardness value is for the specimen. The more amount of Al_2O_3 in the specimen, the more favorable for the hardness value of the specimen In addition, Al_2TiO_5 formed during the spraying process is also a soft phase with low hardness, which is an important factor affecting the hardness of the AT13 coating[30]. As a result, the microhardness values of the AT13 coatings fluctuate.

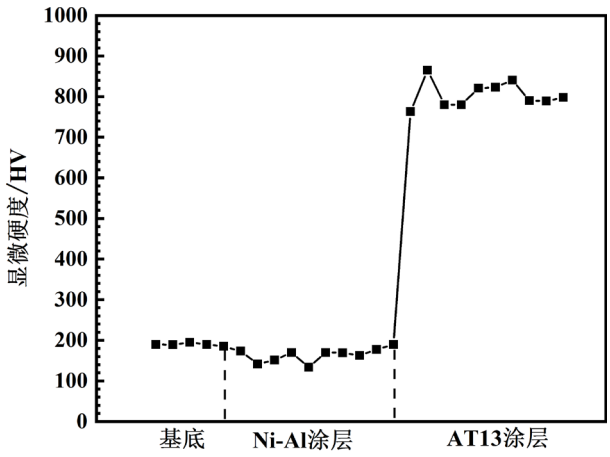

Fig. 9. Microhardness gradient of coatings.

The immersion corrosion test is conducted by artificially creating corrosive environments and conditions so as to conduct corrosion resistance tests on materials. In this experiment, 3.5% NaCl was used as the corrosion medium and the Al_2O_3-13wt.% TiO_2 coatings were subjected to immersion corrosion for 5, 10, 20 and 30 days at room temperature, and after immersion, all the immersed 5, 10, 20, 30 days and un-immersed Al_2O_3-13wt.% TiO_2 coatings were subjected to electrochemical tests. Fig. 10 shows the Potentiodynamic polarization curves of Al_2O_3-13wt.% TiO_2 coatings in different immersion times. The more positive the self-corrosion potential is, the stronger the corrosion resistance of the Al_2O_3-13wt.% TiO_2 coating[31]. The higher corrosion current density represents the faster corrosion rate of the coating[32]. The unimmersed Al_2O_3-13wt.% TiO_2 coating has the most positive self-corrosion potential, indicating that the unimmersed Al_2O_3-13wt.% TiO_2 coating has the strongest corrosion resistance. The coating after 30 days of immersion has the most negative self-corrosion potential, and the Al_2O_3-13wt.% TiO_2 coating after 30 days of immersion has the worst corrosion resistance. The self-corrosion potential of the AT13 coating immersed for 20 days is larger than that of the AT13 coating immersed for 10 days, which is due to the accumulation of corrosion products on the surface of the coating after 20 days of immersion, which blocks the pores of the coating, and makes the The exchange of substances with the corrosive medium inside the coating was affected, so the corrosion resistance of the AT13 coating after 20 days of immersion was stronger than that of the coating after 10 days of immersion.

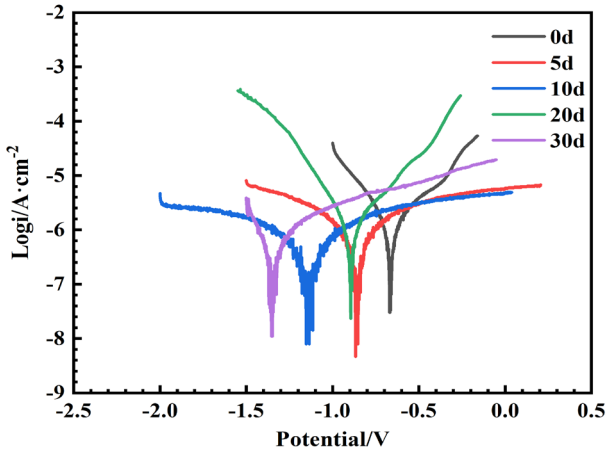

Fig. 10. Potentiodynamic polarization curves of Al_2O_3-13wt.% TiO_2 coating at different immersion times.

Fig. 11 illustrates the surface micro-morphology of Al_2O_3-13wt.% TiO_2 coating immersed in different times. Al_2O_3-13wt.% TiO_2 coating at the beginning of the immersion, no obvious change. After 10 days of immersion white corrosion products started to be produced. This white substance is $Al(OH)_3$, this is because TiO_2 is a very stable compound, it is not easy to react with other substances under normal temperature, it has good stability, γ-Al_2O_3 is a substable phase, when it is in the environment of acid or alkali, γ-Al_2O_3 will react with it. The white corrosion product $Al(OH)_3$ is produced as follows:

$$Al_2O_3 + 6Cl^- = 2AlCl_3 + 3O^{2-}$$
$$O^{2-} + H_2O = 2OH^-$$
$$AlCl_3 + 3(OH)^- = Al(OH)_3 + 3Cl^-$$

When $Al(OH)_3$ is generated, it will fill the pores of the AT13 coating, reduce the porosity of the coating, and be able to block the diffusion of Cl^- into the substrate. For example, the corrosion resistance of the AT13 coating immersed for 20 days was superior to that of the AT13 coating immersed for 10 days. Even though the $Al(OH)_3$ attached to the surface of the AT13 coating prevents a portion of the corrosive solution from entering the interior of the coating, Cl^- will gradually corrode the AT13 coating through the defective locations. Therefore, the corrosion resistance of the AT13 coating gradually deteriorates with increasing immersion time. In addition, also due to the coating has a bimodal distribution structure, part of the melting zone will be corroded preferentially, which will cause the Al_2O_3-13wt.% TiO_2 coating to fail beyond a certain time. In order to extend the service life of the Al_2O_3-13wt.% TiO_2 coating, it can be treated by sealer or laser remelting technology.

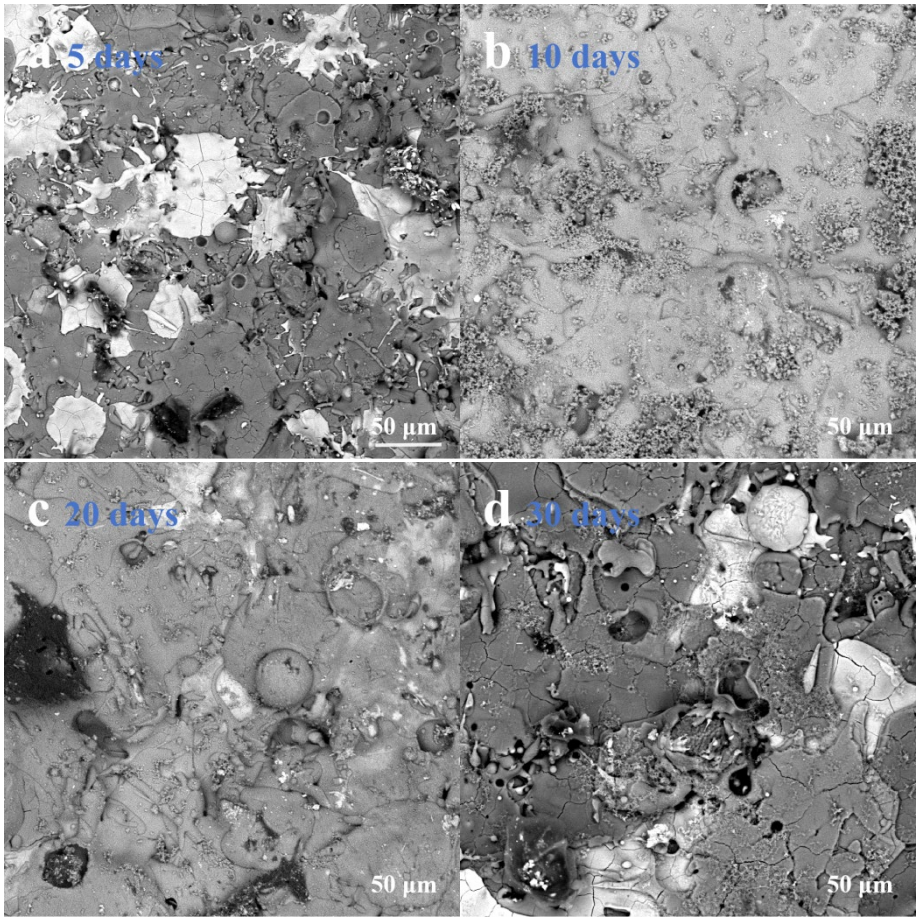

Fig. 11. Surface morphology of Al_2O_3-13 wt.% TiO_2 coating after different immersion times.

4. Conclusion

In this study, Al_2O_3-13wt.% TiO_2 coatings were successfully prepared by APS. The overall morphology of coatings was smooth, the coatings showed a bimorphic structure with fully and partially molten zones, and the cross-sectional view of the coating showed a laminar distribution, which is a typical morphology of PS. Physical phase composition of Al_2O_3-13wt.% TiO_2 coating compared to powder and a part of the α-Al_2O_3 phase was transformed into the γ-Al_2O_3 phase, and a new phase of Al_2TiO_5 was generated by the reaction of Al_2O_3 with the TiO_2 phase. According to the confocal images of the Al_2O_3-13wt.% TiO_2 coatings, the thickness of the coatings is relatively uniform, and their surface roughness value is 5.07 μm. The average hardness of the Al_2O_3-13wt.% TiO_2 coatings is 801 $HV_{0.2}$, and since the coatings show a bimodal distribution structure, the hardness value of the Al_2O_3-13wt.% TiO_2 coatings has a certain ups and downs. The hardness in the fully molten region is higher than that in the partially molten region, α-Al_2O_3 has a higher hardness than the γ-Al_2O_3 phase, and Al_2TiO_5 is the softer phase with lower hardness. After 5, 10, 20 and 30 days of immersion, the Al_2O_3-13wt.% TiO_2 coatings showed no phenomena such as flaking, and there was an accumulation of corrosion products $Al(OH)_3$ on the surface, which indicated that the Al_2O_3-13wt.% TiO_2 coatings had a certain degree of corrosion resistance.

Acknowledgements

The project was supported by New Energy Vehicle Intelligent Network Technology Shandong Province Higher Education Institutions Future Industry Engineering Research Centre.

References

[1] T. Huang, P. Song, Q. Ji, R. Zhai, Y. Huang, B. Zheng and J. Yi, Ceramics International **45**(16), 19856(2019); http://10.1016/j.ceramint.2019.06.241.
[2] C. Li, Y. Li, J. Shi, B. Li, Y. Li, Y. Gao, S. Zhao, R. Goei and A. I. Yoong Tok, Materials Today Communications **31** 103257(2022); http://10.1016/j.mtcomm.2022.103257.
[3] M. Akhtari Zavareh, A. A. D. M. Sarhan, R. Karimzadeh and R. S. A. l. K. Singh, Ceramics International **44**(6), 5967(2018); http://10.1016/j.ceramint.2017.12.175.
[4] P. Shi, H. Sun, G. Yi, W. Wang, S. Wan, Y. Yu and Q. Wang, Ceramics International **49**(11), 18662(2023); http://10.1016/j.ceramint.2023.02.243.
[5] L. Guo, Y. Zhang, F. Wang, Z. Xin, G. Wang and J. Jiang, Materials & Design **247** 113444(2024); http://10.1016/j.matdes.2024.113444.
[6] Z. Cui, Z. Lu, L. Huang, Z. Xu, Z. Wang, W. Duan, H. Che, B. Gou, Q. Liang, J. Huang and X. Chen, Ceramics International 2024); http://10.1016/j.ceramint.2024.12.347.
[7] Z. Li, J. Dong, Y. Yang, J. Sun, K. Yu and Z. Luo, Surface and Coatings Technology **491** 131192(2024); http://10.1016/j.surfcoat.2024.131192.
[8] H. Yan, W. Liu, Y. Ma, T. Wang, L. Wu, L. Yang and S. Tang, Journal of Materials Engineering and Performance **33**(4), 1862(2023); http://10.1007/s11665-023-08093-z.

[9] C. Cheng, T. Lv, B. Song, Y. Chai, J. Luo, G. Li, L. Yang and Y. Zhou, Surfaces and Interfaces **53** 105050(2024); http://10.1016/j.surfin.2024.105050.
[10] I. Shakhova, E. Mironov, F. Azarmi and A. Safonov, Ceramics International **43**(17), 15392(2017); http://10.1016/j.ceramint.2017.08.080.
[11] H. Zhang, K. Chong, W. Zhao and Z. Sun, Surface and Coatings Technology **344** 163(2018); http://10.1016/j.surfcoat.2018.03.021.
[12] M. Rafiei, H. Ghayour, H. Mostaan and M. Zavaran Hosseini, Journal of Materials Processing Technology **266** 569(2019); http://10.1016/j.jmatprotec.2018.11.037.
[13] J. J. Li, Y. F. Zhang, Q. Li, X. Y. Ran, Q. Hao and X. L. Guo, Digest Journal of Nanomaterials and Biostructures **19**(1), 1(2024); http://10.15251/djnb.2024.191.1.
[14] R. Taurino, S. Martinuzzi, E. Padovano, S. Caporali and F. Bondioli, Journal of the European Ceramic Society **45**(5), 117133(2025); http://10.1016/j.jeurceramsoc.2024.117133.
[15] A. Khanna, D. G. Bhat, A. Harris and B. D. Beake, Surface and Coatings Technology **201**(3-4), 1109(2006); http://10.1016/j.surfcoat.2006.01.033.
[16] Y. Yuanzheng, Z. Youlan, L. Zhengyi and C. Yuzhi, Materials Science and Engineering:A **291**(1), 168(2000); http://10.1016/S0921-5093(00)00983-7.
[17]S. Tailor and A. Modi, CeramicsInternational (2024); http://10.1016/j.ceramint.2024.11.478.
[18] Y. Dai, J. Zou, X. Ning, H. Wei and F. Li, Colloids and Surfaces A: Physicochemical and Engineering Aspects **697** 134420(2024); http://10.1016/j.colsurfa.2024.134420.
[19] W. Wang, D. Ren, X. Zhang, W. Du, S. Zhu and H. Li, Ceramics International **50**(8), 13388(2024); http://10.1016/j.ceramint.2024.01.251.
[20] K. Chen, P. Song, C. Li, Y. Zhou, X. He, X. Yu and J. Lu, Ceramics International **44**(12), 13727(2018); http://10.1016/j.ceramint.2018.04.214.
[21] M. Hashemzadeh, K. Raeissi, F. Ashrafizadeh, F. Simchen, A. Hakimizad, M. Santamaria and T. Lampke, Transactions of Nonferrous Metals Society of China **34**(10), 3326(2024); http://10.1016/s1003-6326(24)66611-2.
[22] Y. Wang, Y. Guo and Q. Zhang, Materials Today Communications **44** 112182(2025); http://10.1016/j.mtcomm.2025.112182.
[23] E. Klyatskina, E. Rayón, G. Darut, M. D. Salvador, E. Sánchez and G. Montavon, Surface and Coatings Technology **278** 25(2015); http://10.1016/j.surfcoat.2015.07.029.
[24] L. Łatka, M. Szala, M. Nowakowska, M. Walczak, T. Kiełczawa and P. Sokołowski, Surface and Coatings Technology **455** 129180(2023); http://10.1016/j.surfcoat.2022.129180.
[25] K. Zhang, Z. Zhou, L. Wu, G. Wang and X. Zhang, Ceramics International **49**(18), 30522(2023); http://10.1016/j.ceramint.2023.07.002.
[26] Y. Wang, C. G. Li, W. Tian and Y. Yang, Applied Surface Science **255**(20), 8603(2009); http://10.1016/j.apsusc.2009.06.033.
[27] J. Jiang, W. Wang, X. Zhao, Y. Liu, Z. Cao and P. Xiao, Engineering Fracture Mechanics **196** 191(2018); http://10.1016/j.engfracmech.2018.04.031.
[28] J. Jiang, L. Jiang, Z. Cai, W. Wang, X. Zhao, Y. Liu and Z. Cao, Surface and Coatings Technology **357** 433(2019); http://10.1016/j.surfcoat.2018.10.020.
[29] J. J. Li, Y. F. Zhang, Q. Li, Q. Hao, X. Y. Ran and X. L. Guo, Digest Journal of Nanomaterials and Biostructures **18**(4), 1275(2023); http://10.15251/djnb.2023.184.1275.

[30] H. Luo, D. Goberman, L. Shaw and M. Gell, Materials Science and Engineering **A346** 237(2003); http://10.1016/S0921-5093(02)00523-3.
[31] K. Yu, W. Zhao, Z. Li, B. Zhang, G. Xiao and H. Zhang, Surface and Coatings Technology **458** 129352(2023); http://10.1016/j.surfcoat.2023.129352.
[32] K. Rahmani, G. H. Majzoobi, H. Bakhtiari and A. Sadooghi, Materials Chemistry and Physics **271** 124946(2021); http://10.1016/j.matchemphys.2021.124946.